IEEE Access
Multidisciplinary ⋮ Rapid Review ⋮ Open Access Journal

Received 17 June 2022, accepted 4 July 2022, date of publication 12 July 2022, date of current version 29 July 2022.

Digital Object Identifier 10.1109/ACCESS.2022.3189992

RESEARCH ARTICLE

Multiturn Planar Inductor for the Improvement of Signal-to-Noise Ratio Response in Magnetic Resonance Microscopy

BYUNG-PAN SONG[1], HYEONG-SEOP KIM[2], SUNG-JUN YOON[3], DANIEL HERNANDEZ[4], KYOUNG-NAM KIM[4], AND SEUNG-KYUN LEE[1,2]

[1]Department of Biomedical Engineering, Sungkyunkwan University, Suwon, Gyeonggi-do 16419, South Korea
[2]Department of Intelligent Precision Healthcare Convergence, Sungkyunkwan University, Suwon, Gyeonggi-do 16419, South Korea
[3]Department of Electronic and Electrical Engineering, Sungkyunkwan University, Suwon, Gyeonggi-do 16419, South Korea
[4]Department of Biomedical Engineering, Gachon University, Yeonsu-gu, Incheon 21936, South Korea

Corresponding authors: Kyoung-Nam Kim (kyoungnam.kim@gachon.ac.kr) and Seung-Kyun Lee (lee.seungkyun@gmail.com)

This work was supported in part by the Korean Brain Research Institute (KBRI) Basic Research Program through the KBRI funded by the Ministry of Science and ICT (MSIT) under Grant 22-BR-05-02, and in part by the National Research Foundation of Korea (NRF) funded by the MSIT under Grant 2019R1A2C1006448.

ABSTRACT In this study, we propose a novel, multiturn histology coil for microscopic magnetic resonance (MR) imaging of histological tissue slices with substantially higher signal-to-noise-ratio (SNR) outcomes compared with previously developed coils. We performed electromagnetic simulations of the proposed coils and acquired MR images from a gelatin phantom and a rat brain slice with the implemented coils. The performances of the coils were evaluated by comparing the measured and simulated radio-frequency transmission (B_1^+) fields in a flip-angle map form, and with low flip-angle gradient echo images to calculate the SNR increase as a function of the number of turns (n) of the coils. This study was performed on a 3 T MR imaging system. The proposed coil with $n = 7$ achieved SNR greater than 3.5 times that of a single-turn coil while preserving the highly uniform B_1^+ field across the imaging region. The proposed method provides new possibilities for high-resolution MR imaging of microscopic tissue samples for biomedical applications.

INDEX TERMS Magnetic resonance imaging (MRI), microscopy, signal-to-noise ratio (SNR), radiofrequency (RF), multiturn planar inductor (MTPI).

I. INTRODUCTION

Microscopic tissue imaging with magnetic resonance imaging (MRI) can be used for high-resolution measurements of magnetic resonance properties of biological tissues that can be compared directly with optical images [1]–[4]. These types of investigations can help elucidate the origin of MRI contrast observed in vivo [5]–[7]. Owing to the small number of proton spins in microscopic tissue sample volumes, the signal-to-noise ratio (SNR) is low in MR microscopy. Extensive research has been conducted on the design of radiofrequency (RF) coils for MR microscopy [8], and several types of coils have been proposed, including surface [9], [10], flat-histology [3], birdcage [11], Helmholtz [12], and solenoid coils [1], [13]–[18]. Among these, the flat histology coil based on a single-turn inductor [3] and the solenoid coil have a high filling factor, high uniformity of RF transmission (B_1^+) field, and high SNR within the imaging volume. In particular, the histology coil is specifically designed to image a flat sample (such as a common histology slice) within a compact space. This coil type has been successfully used to image Alzheimer's disease brain specimens with high spatial resolution [5], [19].

One difference between the histology coil and a conventional solenoid coil is that the former has a considerably lower resistance owing to its relatively large cross-section and short transport length of the RF current flow through this coil. While this reduces the coil's Nyquist noise at room

The associate editor coordinating the review of this manuscript and approving it for publication was Chun-Hsing Li.

temperature, it increases the possibility that the noise from the RF circuitry downstream from the coil itself may dominate the intrinsic noise of the coil. Given that the sample noise from a microscopic sample is usually negligible, this implies that the RF-circuit noise can be the limiting factor in the SNR of the histology coil.

In this study, we demonstrate that the SNR of a histology coil can be significantly increased by combining the features of the solenoid coil (multiturn) and the original histology coil (flat geometry). The resulting coil, which is called hereafter a ''multiturn planar inductor (MTPI)'', maintains a high filling factor and B_1^+ homogeneity for a flat sample, and achieves high SNR by increasing the inductance (L) of the coil through multiple turns ($n > 1$) to increase the detection sensitivity for the sample's MR signal. We designed and manufactured the MTPI and demonstrated its performance in a 3.0 T clinical scanner, in comparison with an original, single-turn planar inductor. The number of turns was varied ($n = 3, 5, 7$). Considerably higher SNR values were obtained for all the configurations with $n > 1$ than those for $n = 1$, but the SNR improvement showed evidence for saturation as n increased. These findings are consistent with the coil noise dominance at large n.

II. MATERIALS AND METHODS

A. THEORY OF MTPI

In MR microscopy, a flat histology coil is more efficient than conventional surface coils. However, the SNR can be further improved by shifting to the MTPI design. To achieve this, the inductance L of the coil and the sensitivity to the sample's MR signal need to increase while maintaining a homogeneous B_1^+ and high filling factor. In a multiturn design, as in a solenoid, the coil's L is proportional to the square of the number of turns (n), and the MR signal induced in the coil increases in proportion to n [13], [20]–[22]. However, when n increases, the cross-section of each conductor decreases because multiple turns must be manufactured within a fixed surface; in addition, the conductor length increases in proportion to n [23]. Accordingly, the resistance of the RF coil increases in proportion to n^2. The SNR improvement cannot be achieved by merely increasing L owing to the quality factor Q, which affects the SNR change (Q is proportional to L and inversely proportional to the resistance R, both of which are proportional to n^2) [24]. However, noise sources exist in signal paths following the coil, such as in the preamplifier, coaxial cable used to connect the coil to the MR system, and in the reception circuitry. The noise in the receiver chain, which is usually neglected in the general scanning process when the detected signal is abundant, dominates the noise term in microscale tissue imaging, wherein the signal is insufficient [25], [26]. The SNR of the MTPI based on considerations of the receiver chain noise can be expressed as [25]

$$\mathrm{SNR} \approx \frac{nS}{\sqrt{n^2N_s^2 + n^2N_c^2 + N_r^2}} \approx \frac{nS}{\sqrt{n^2N_c^2 + N_r^2}}, \quad (1)$$

where n is the number of turns, and S is the MR signal from spins. N_s is the noise from the sample that depends on its electrical properties. Given that microscale samples are considered, N_s can be neglected. nN_c is the thermal noise of the coil, and N_r is the receiver chain noise. The linear dependence of the coil noise on n follows from the fact that the coil noise scales as $\sqrt{R}$ and $R \propto n^2$, as discussed above. According to Eq. (1), if N_r^2 is larger than $n^2N_c^2$, it would set the limit of the SNR. This study hypothesizes that a conventional flat histology coil (which can be viewed as an MTPI with $n = 1$) is in receiver chain-dominated regime and proposes an MTPI design with $n > 1$ to approach coil noise ($n^2N_c^2$) dominance for improving SNR in microscopic imaging. Note that in for a considerably large n, the SNR expressed in Eq. (1) will saturate to a limiting value, S/N_c. In such a case, the complexity of the coil design and parasitic losses will disfavor further increase of n.

B. MTPI SIMULATIONS

To verify that the proposed coils can produce uniform magnetic fields for a slim sample, we conducted electromagnetic simulations using a commercial finite-difference time-domain solver software (Sim4Life, Zurich, Switzerland). The simulations were conducted at a frequency of 123.25 MHz corresponding to the Larmor frequency at 3 T. The design consisted of individual coils with one, three, five, and seven turns. The sample was a cylindrical phantom with a radius of 12 mm and height of 1 mm, with chemical solutions that emulated the electrical properties of muscle (permittivity of 63.56 and conductivity of 0.718 S/m) [27]. The coil volume for the inductor line was $30 \times 4 \times 45$ mm^3. The separation distances between the lines were set to 1 mm for all the coils, and the thicknesses of the lines for the coils with one, three, five, and seven turns were set as 30, 9, 5 and 3.3 mm respectively. The simulation designs are shown in Figure 1. The conductor lines were set as perfect electrical conductors. Two layers of Plexiglass with permittivity of 3.4 were used to improve the field uniformity.

C. MTPI DESIGN AND MANUFACTURING

All the coils consisted of two parts (resonator and matching circuit). The resonator of the histology coil [2], [4] has a highly homogeneous B_1^+ field and a large filling factor. In [4] the coil consisted of a U-shaped copper conductor with a Teflon insert that operate as a parallel capacitance. We propose a new coil design to improve the SNR while maintaining the innate advantages of a histology coil. The histology coil [2], [4] was remanufactured by expanding the internal space to fit our experimental setup without changing the material and was then compared with the multiturn coils. The histology coil used for comparison was the coil used in [4] without any modification. The lengths of both the multiturn and histology coils were set to 45 mm to ensure that they had the same dimensions. The design of the multiturn coil involved multiple conductors turns (3, 5, and 7) wound on flat and thin cuboidal shaped cavities to increase their sensitivity

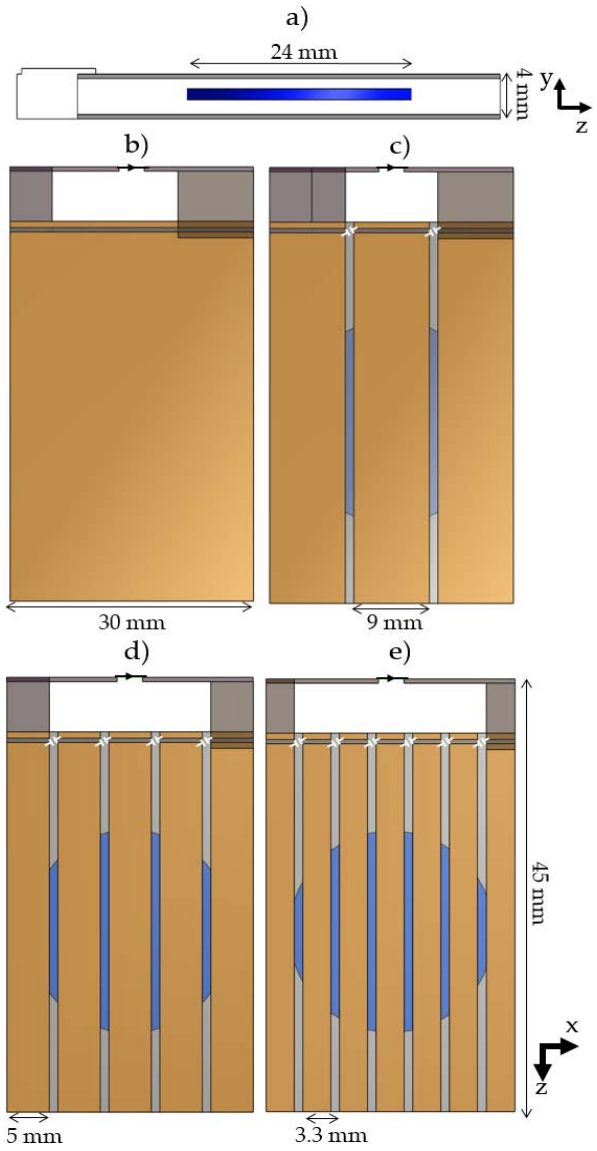

FIGURE 1. Design of the simulated coil with phantom in the a) z–y and z–x planar views for b) one-, c) three-, d) five-, and e) seven- turn coils.

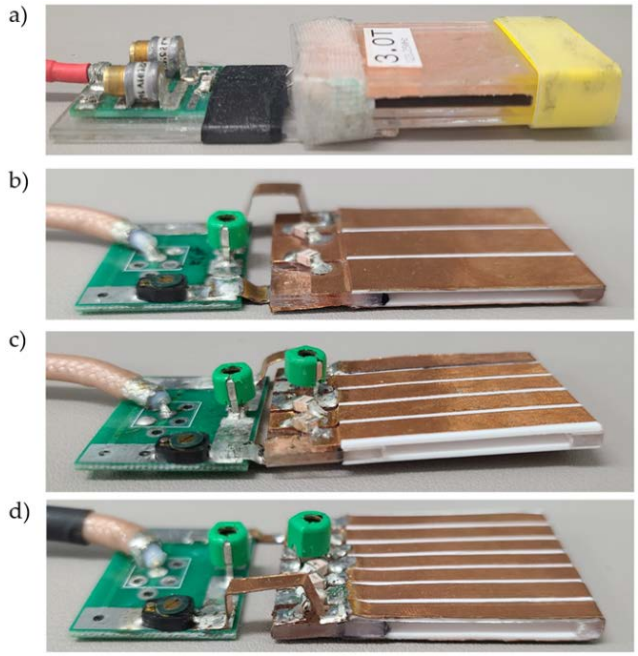

FIGURE 2. Manufactured coils with a) one, b) three, c) five, and d) seven turns.

to proton spin signals by increasing the L of the coil. The matching circuit that performed impedance matching with the MR system and fine adjustment of the resonance frequency consisted of a parallel and series capacitor for all the coils. The matching circuits of all the coils were connected to the MRI system via a 7 cm coaxial cable (K0225D-08, Huber and Suhner, Herisau, Switzerland) and BNC connector. The housings of the coils were manufactured with polypropylene plates, and plexiglass bridges and spacers. Plexiglass spacers must be placed underneath the tuning capacitors to maintain a homogeneous B_1^+ distribution. The presence of this spacer provided both additional capacitance and allowed for the current to be spread homogeneously throughout the strip before the field-of-view (FOV) was reached from the soldered parts of tuning capacitors [2], [4]. Teflon was used for the spacers in previous studies [2], [4]. However, plexiglass was used instead of Teflon because of its higher dielectric constant (Teflon: 2.1, Plexiglass: 3.4); this introduces an advantage in terms of the added capacitance and simplifies the manufacturing process. Figure 2 shows the coils, matching circuits, and frame which were applied to all multiturn coils.

All the resonators were constructed by winding a copper strip in the frame (thickness: 0.06 mm). The width of the strip was changed according to the number of turns to cover the fixed volume while it minimized the gap and maximized the strip's cross-sectional area. The copper strips in each turn were arranged parallel to each other (running in the z-direction), and tuning capacitors were connected to the next strip at the plexiglass spacer region. Care was taken to have the gaps between adjacent strips minimized to achieve a homogeneous distribution of B_1^+ in the cavity of the coil. The resonators were tuned to the resonant frequency (123.25 MHz) with tuning capacitors (Johanson Dielectrics Inc., Camarillo, CA, USA) such that the n-turn coil had $n - 1$ tuning capacitors, placed in the space between the copper lines, as shown in Figure 1.

D. MRI SCAN

For the B_1^+ map evaluations, a gelatin phantom was constructed by filling gelatin solution in a three-dimensionally printed housing which fitted in the cavities of the coils. The gelatin phantom was a cuboid with a 20 mm square side (in plane) and a thickness of 0.4 mm. For the demonstration of actual histological sample imaging, a formalin-fixed rat brain slice (thickness: 40 μm) was mounted between two glass slides with respective thicknesses equal to 1 mm and 0.17 mm. All animal research protocols were approved by

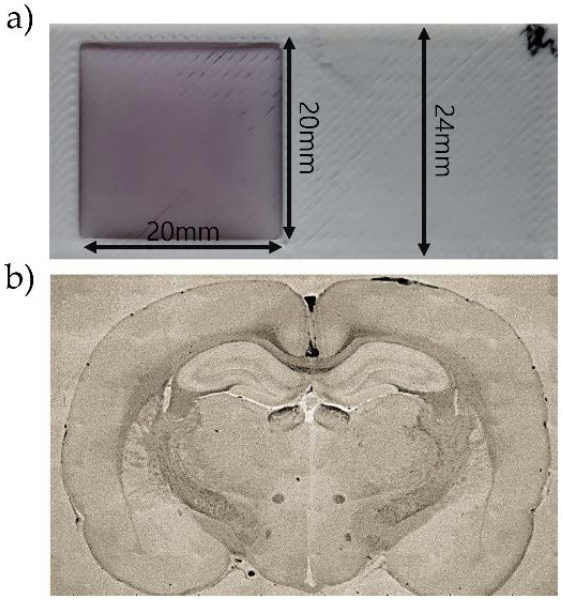

FIGURE 3. Samples used for MTPI coil evaluation and MR imaging. a) Gelatin sample and b) the optical image of a fixed coronal rat brain slice (thickness: 40 μm).

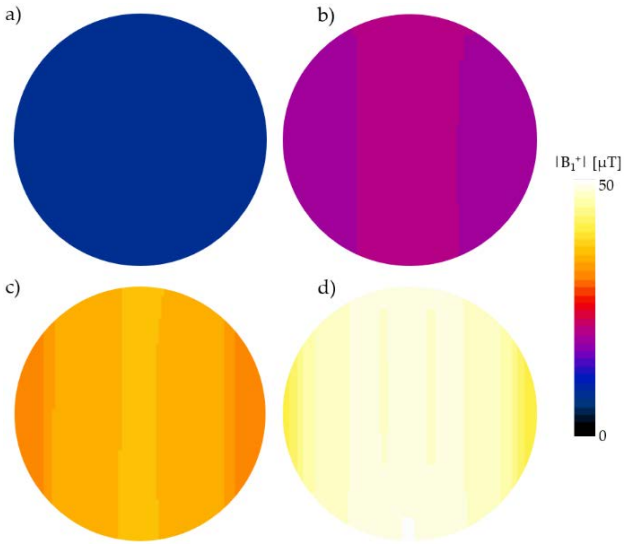

FIGURE 4. Simulated B_1^+ maps inside the phantom for the a) one, b) three, c) five and d) seven-turn coils.

TABLE 1. Radiofrequency coil (RF) bench-test outcomes.

Label	S_{11} [dB]	UQ	LQ		Impedance [Ω]	Q-ratio
			Gelatin	Rat brain		Rat brain
1-turn	−37.45	110.4	110.3	110.3	49.485	1.0009
3-turns	−33.23	181.9	181.7	181.6	50.635	1.0017
5-turns	−42.69	214.1	213.7	213.8	50.331	1.0014
7-turns	−38.23	231	228.4	229.2	49.668	1.0079

the Sungkyunkwan University Institutional Animal Care and Use Committee (IACUC). Clear nail varnish was used to maintain the brain slice in place and prevent its dehydration. Figure 3 shows the optical image of the histology slide and gelatin phantom used in this experiment.

All images were obtained in a clinical 3 T MRI (Magnetom Prisma, Siemens Healthineers, Erlangen, Germany). The B_1^+ map was obtained by SA2RAGE fast B_1^+ mapping sequence [28] with a repetition time (TR) = 5 ms, echo time (TE) = 2.35 ms, flip angle = 8° matrix = 96 × 128, pixel size = 0.5234 × 0.5234 mm^2, bandwidth = 400 Hz/pixel, averages = 1, and scan time = 0.49 s. To compare coil SNR values, the gelatin phantom was imaged with a fast low-angle shot (FLASH) sequence with the following parameters: TR = 50 ms, TE = 5.3 ms, matrix size = 168 × 224, pixel size = 0.1786 × 0.1786 mm^2, bandwidth = 210 Hz/pixel, averages = 32, scan time = 4 min and 28 *s*. To compare histology sample images, rat-brain histological slices were imaged with the FLASH sequence with the following parameters: TR = 30 ms, TE = 5.3 ms, matrix size = 168 × 224, pixel size = 0.1562 × 0.1562 mm2, bandwidth = 210 Hz/pixel, averages = 32. The total scan took 2 min and 41 s. The flip angles were optimized to the Ernst angle [29] for the imaging of the gelatin sample and rat-brain slice. The flip angle denotes the degree of spin excitation by an RF pulse. The RF pulse tilts the spins aligned along the static magnetic field to the transverse (xy)-plane. The amount of tilting is referred to as the flip angle.

III. RESULTS

A. SIMULATIONS

We computed the B_1^+ field for the simulated coils with one, three, five, and seven turns to verify the field uniformity for a circular numerical phantom. The B_1^+ field maps normalized to an input power of 1 W are shown in Figure 4. The coil with one and three turns had a mean of 6.6 and 19 μT, while the standard deviations were 0.07 and 0.05 μT, respectively. Meanwhile, the mean and standard deviation values of the field acquired with the five-turn coil were 33 and 0.11 μT, respectively. By contrast, the coil with seven turns had mean and standard deviation values equal to 46 and 0.22 μT, respectively. These results are expected because the seven-turn coil has more current lines running across the phantom than the coil with five turns; in this respect, it can produce a stronger and more uniform field.

B. MTPI BENCH TEST

Table 1 lists the reflection mode measurements, which were obtained using a network analyzer (E5063A, Keysight, Santa Rosa, CA, USA). The S-parameter spectra were measured at the terminal point of the BNC connector connected with the matching circuit via a coaxial cable. The Q-values were measured based on the reflection-mode method [30]. The ratio between the loaded and unloaded quality factors is called the *Q-ratio* (*UQ*/*LQ*); it is determined by the coil resistance and resistance induced from the sample ($Q\text{-}ratio = (R_{coil} + R_{sample}) \ / \ R_{coil}$). Therefore, *Q-ratio* values less than two indicate that the coil noise dominates the sample noise [31].

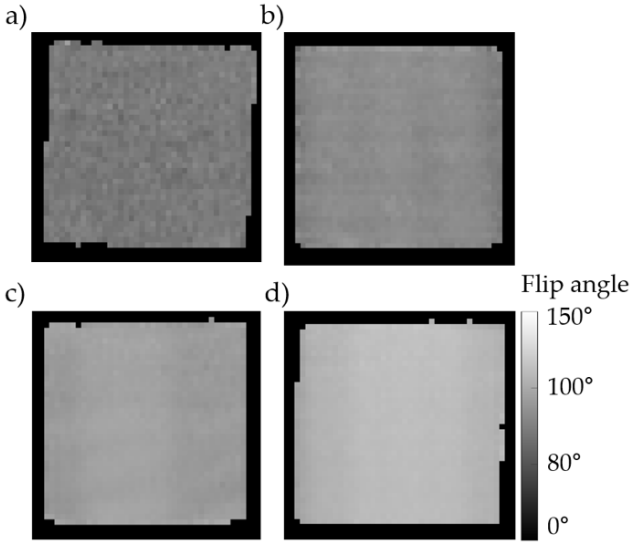

FIGURE 5. B_1^+ maps represented as flip angle maps for all tested coils. a-d) Single-, three-, five-, and seven-turn coils.

TABLE 2. Mean values and standard deviation of flip angle.

Label	Mean [°]	Standard deviation [°]	Percentage [%]
1-turn	71.47	3.75	5.25
3-turns	81.13	3.11	3.83
5-turns	92.79	2.85	3.07
7-turns	93.35	3.27	3.50

All coils had *Q-ratio* values less than two, which is expected from the significantly small sample size. This indicates that the *Q*-value does not change considerably even when various samples are loaded, which presents an advantage that coil retuning is not necessary when imaging multiple samples with one coil.

The symbol S_{11} denotes the loss rate of power in the entire RF-coil circuit as shown in Table 1. Conversion of the loss rates of all tested coils in percentage values yielded: single-turn: 0.018 %, three-turn: 0.048 %, five-turn: 0.005 %, and seven-turn: 0.015 %.

C. B_1^+ FIELD DISTRIBUTION

The measured B_1^+ maps represented by the flip angle maps are shown in Figure 5 for all the tested coils. The statistics for the flip angle maps are summarized in Table 2. In all the coils, the standard-deviation value of the flip angle inside the phantom was no more than 5.25% of the average value. These results indicate that the B_1^+ field is homogeneous in a large part of the coil cavity.

D. SNR EVALUATION FOR MULTITURN COILS

In addition to the B_1^+ field map, the SNR for each coil was measured on the gelatin and rat-brain phantoms.

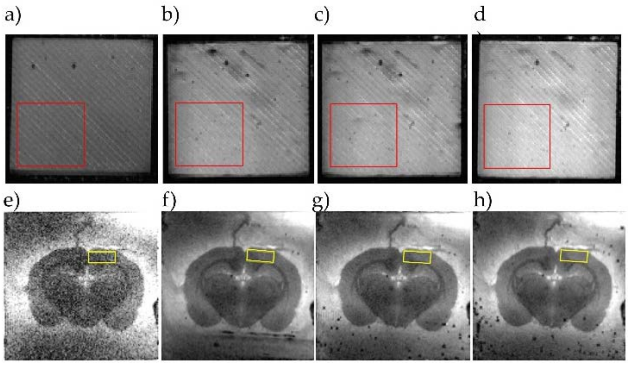

FIGURE 6. (a–d) SNR comparisons of gelatin phantom imaged with the fast low-angle shot (FLASH) sequence. (a) Single-, (b) three-, (c) five-, and (d) seven-turn coils. (e-h) SNR comparisons of rat-brain slice imaged with the FLASH sequence. (e) Single-, (f) three-, (g) five-, and (h) seven-turn coils.

TABLE 3. Signal-to-noise ratios computed from the images acquired with each coil and phantom.

Coil	Gelatin	Rat brain
1-turn	17.04	2.25
3-turns	50.05	6.75
5-turns	54.65	7.31
7-turns	65.64	8.46

The SNR was calculated as the ratio of the mean value of signal intensity in a region-of-interest (ROI) to the root-mean-square value of noise regions in the background (cropped from the displayed images) of the reconstructed images [32]. Figure 6 in the top row shows the images acquired with the gelatin phantom for the coils with one, three, five, and seven turns. As the number of coil turns increases, the SNR tends to increase. Compared with the conventional histology coil, the SNR increased by 2.93-, 3.20-, and 3.85-time in the three-, five-, and seven-turn coil cases. The SNR comparison of the rat-brain slice is shown in the bottom row of Figure 6. Compared with the conventional histology coil, the SNR increased by 3.00-, 3.24-, and 3.76-time in the three-, five-, and seven-turn coil cases. Table 3 summarizes the computed SNR for each coil and the imaging object. These results indicate that the use of a coil of this type with higher turns leads to a higher SNR.

IV. DISCUSSION AND CONCLUSION

In this study, we evaluated specially designed multiturn coils in a clinical 3 T scanner and demonstrated that they were capable of imaging rats brain histological slices. The coil implemented in a prior study (single-turn coil) was redesigned and compared with the multiturn coil [4]. As shown, the multiturn coil improved the SNR by at least 50% and by nearly 300% for $n = 7$. In MR microscopy, the coil has to be minimized to correspond to the sample size for optimizing the filling factor and reducing the thermal noise of the coil components. Simultaneously, because the absolute

signal amount is considerably low, high B_1 homogeneity is required to minimize signal loss.

In general, in scan processes with insufficient signal amounts, a method was used to control the resistance of the coil by increasing the cross-sectional area, or by decreasing the lengths of the coil's conductors. We achieved SNR improvements by increasing the amplitude of the signal received from the coil by increasing L in the cavity of the coil. L was increased by increasing the number of conductors encased in a fixed volume. This reduced the conductor's cross-sectional area and increased the length. These changes caused an increase in the resistance of the entire coil. The SNR performances of the coils indicated that these followed the behavior predicted by Equation (1), where increasing n makes the sample signal and coil noise terms dominating over the receiver-chain-noise term in the denominator. In future experiments, quantitative measurements of $n^2N_c^2$ and N_r^2 can help determine the optimum number of turns of a multiturn coil to maximize SNR.

A unique feature of a flat histology coil in comparison with a surface coil is that the former produces the B_1 field in the plane of the sample. For a microscopically thin sample, this has the advantage that the eddy-current cross section is significantly small so that the E field induced in the sample and specific absorption rate (SAR) are considerably lower than that if B_1 is normal to the plane. Using the geometric parameters used in this work, we estimated that less than 0.1 μW of heat is deposited to the sample if $B_1 = 10$ μT is applied with 10% duty cycle. Even when normalized to the small mass of the sample, this corresponds to a SAR of less than 0.2 W/kg, an order of magnitude lower than typical SAR values in human scans [20]. Based on this, we believe that the temperature of the ex-vivo sample can be easily regulated in scans using the proposed coil.

MR imaging has disadvantages in terms of the resolution compared with optical imaging; however, multiturn coils are extensively utilized in experiments aimed at the collection of information of microscopic tissue that can only be obtained from MRI. Susceptibility anisotropy studies [6] on ex-vivo samples are practical applications. The anisotropies of ex-vivo and in-vivo tissues are different because anisotropy depends on tissue viability. However, in the measurements of the anisotropy in vivo, simultaneous rotation of the coil and body in multiple directions within a confined bore space is impractical. Therefore, ex-vivo susceptibility tensor imaging (STI) studies on various human tissues have been used to study the anisotropy of the human body despite the associated limitations. The wide space of our setup facilitates multiple-orientation imaging [33], [34] as well as the use of physical laboratory equipment, such as a nutrient circulation device, or a humidity control device to maintain tissue life. Our study can, thus, allow the pursuit of tissue bio-magnetic property studies that emulate in-vivo states by extending in-vitro tissue experiments.

The results of the present study demonstrated that the proposed multiturn coils constitute a suitable design for microscopic sample imaging. Considerable gain in SNR (up to 300%) facilitated high-resolution MR microscopy of a histology sample. The results were derived from multiple turns wrapped around a limited volume to reduce the relative contribution of the receive-chain noise inside the MRI, which was the key factor responsible for the SNR improvements. The combination of multiturn coils and large-bore imaging can open up new possibilities for orientation-dependent tissue microstructure and magnetic property imaging.

REFERENCES

[1] R. W. Bowtell, G. D. Brown, P. M. Glover, M. McJury, and P. Mansfield, "Resolution of cellular structures by NMR microscopy at 11.7 T," *Phil. Trans. Roy. Soc. London A*, vol. 333, no. 1632, pp. 457–467, Dec. 1990, doi: 10.1098/rsta.1990.0173.

[2] D. M. Hoang, E. B. Voura, C. Zhang, L. Fakri-Bouchet, and Y. Z. Wadghiri, "Evaluation of coils for imaging histological slides: Signal-to-noise ratio and filling factor," *Magn. Reson. Med.*, vol. 71, no. 5, pp. 1932–1943, May 2014, doi: 10.1002/mrm.24841.

[3] M. D. Meadowcroft, S. Zhang, W. Liu, B. S. Park, J. R. Connor, C. M. Collins, M. B. Smith, and Q. X. Yang, "Direct magnetic resonance imaging of histological tissue samples at 3.0T," *Magn. Reson. Med.*, vol. 57, no. 5, pp. 835–841, May 2007, doi: 10.1002/mrm.21213.

[4] B.-P. Song, H.-S. Kim, K.-N. Kim, and S.-K. Lee, "Inductively coupled RF coil for imaging a 40 μm-thick histology sample in a clinical MRI scanner," *J. Korean Phys. Soc.*, vol. 77, no. 1, pp. 87–93, Jul. 2020, doi: 10.3938/jkps.77.87.

[5] M. D. Meadowcroft, J. R. Connor, M. B. Smith, and Q. X. Yang, "MRI and histological analysis of beta-amyloid plaques in both human Alzheimer's disease and APP/PS1 transgenic mice," *J. Magn. Reson. Imag.*, vol. 29, no. 5, pp. 997–1007, May 2009, doi: 10.1002/jmri.21731.

[6] E. Kaden, N. G. Gyori, S. U. Rudrapatna, I. Y. Barskaya, I. Dragonu, M. D. Does, D. K. Jones, C. A. Clark, and D. C. Alexander, "Microscopic susceptibility anisotropy imaging," *Magn. Reson. Med.*, vol. 84, no. 5, pp. 2739–2753, Nov. 2020, doi: 10.1002/mrm.28303.

[7] J. P. Marques, R. Maddage, V. Mlynarik, and R. Gruetter, "On the origin of the MR image phase contrast: An *in vivo* MR microscopy study of the rat brain at 14.1 T," *NeuroImage*, vol. 46, no. 2, pp. 345–352, Jun. 2009, doi: 10.1016/j.neuroimage.2009.02.023.

[8] T. Neuberger and A. Webb, "Radiofrequency coils for magnetic resonance microscopy," *NMR Biomed.*, vol. 22, no. 9, pp. 975–981, Nov. 2009, doi: 10.1002/nbm.1246.

[9] J. J. Flint, C. H. Lee, B. Hansen, M. Fey, D. Schmidig, J. D. Bui, M. A. King, P. Vestergaard-Poulsen, and S. J. Blackband, "Magnetic resonance microscopy of mammalian neurons," *NeuroImage*, vol. 46, no. 4, pp. 1037–1040, Jul. 2009, doi: 10.1016/j.neuroimage.2009.03.009.

[10] R. J. A. Nabuurs, I. Hegeman, R. Natté, S. G. van Duinen, M. A. van Buchem, L. van der Weerd, and A. G. Webb, "High-field MRI of single histological slices using an inductively coupled, self-resonant microcoil: Application to *ex vivo* samples of patients with Alzheimer's disease," *NMR Biomed.*, vol. 24, no. 4, pp. 351–357, 2011, doi: 10.1002/nbm.1598.

[11] W. U. Roffmann, S. Crozier, K. Luescher, and D. M. Doddrell, "Small birdcage resonators for high-field NMR microscopy," *J. Magn. Reson., B*, vol. 111, no. 2, pp. 174–177, May 1996, doi: 10.1006/jmrb.1996.0077.

[12] S. E. Hurlston, W. W. Brey, S. A. Suddarth, and G. A. Johnson, "A high-temperature superconducting Helmholtz probe for microscopy at 9.4 T," *Magn. Reson. Med.*, vol. 41, no. 5, pp. 1032–1038, May 1999, doi: 10.1002/(SICI)1522-2594(199905)41:5<1032::AID-MRM23>3.0.CO;2-X.

[13] V. Vegh, P. Gläser, D. Maillet, G. J. Cowin, D. C. Reutens, "An implantable RF solenoid for magnetic resonance microscopy and microspectroscopy," *IEEE Trans. Biomed. Eng.*, vol. 59, no. 8, pp. 2118–2125, Aug. 2012, doi: 10.1109/TBME.2011.2178239.

[14] V. Vegh, P. Gläser, D. Maillet, G. J. Cowin, and D. C. Reutens, "High-field magnetic resonance imaging using solenoid radiofrequency coils," *Magn. Reson. Imag.*, vol. 30, no. 8, pp. 1177–1185, Oct. 2012, doi: 10.1016/j.mri.2012.04.027.

[15] K. Jasiński, A. Młynarczyk, P. Latta, V. Volotovskyy, W. P. Włglarz, and B. Tomanek, "A volume microstrip RF coil for MRI microscopy," *Magn. Reson. Imag.*, vol. 30, no. 1, pp. 70–77, Jan. 2012, doi: 10.1016/j.mri.2011.07.010.

[16] A. Arbabi, L. S. Noakes, D. Vousden, J. Dazai, S. Spring, O. Botelho, T. Keshavarzian, M. Mattingly, J. E. Ellegood, L. M. J. Nutter, R. Wissmann, J. G. Sled, J. P. Lerch, R. M. Henkelman, and B. J. Nieman, "Multiple-mouse magnetic resonance imaging with cryogenic radiofrequency probes for evaluation of brain development," *NeuroImage*, vol. 252, May 2022, Art. no. 119008, doi: 10.1016/j.neuroimage.2022.119008.

[17] M. Sack, F. Wetterling, A. Sartorius, G. Ende, and W. Weber-Fahr, "Signal-to-noise ratio of a mouse brain13C CryoProbe system in comparison with room temperature coils: Spectroscopic phantom and*in vivo* results," *NMR Biomed.*, vol. 27, no. 6, pp. 709–715, Jun. 2014, doi: 10.1002/nbm.3110.

[18] D. L. Olson, T. L. Peck, A. G. Webb, R. L. Magin, and J. V. Sweedler, "High-resolution microcoil 1 H-NMR for mass-limited, nanoliter-volume samples," *Science*, vol. 270, no. 5244, pp. 1967–1970, Dec. 1995, doi: 10.1126/science.270.5244.1967.

[19] M. D. Meadowcroft, D. G. Peters, R. P. Dewal, J. R. Connor, and Q. X. Yang, "The effect of iron in MRI and transverse relaxation of amyloid-beta plaques in Alzheimer's disease," *NMR Biomed.*, vol. 28, no. 3, pp. 297–305, Mar. 2015, doi: 10.1002/nbm.3247.

[20] D. Hernandez and K. N. Kim, "A review on the RF coil designs and trends for ultra high field magnetic resonance imaging," *Investig. Magn. Reson. Imag.*, vol. 24, no. 3, pp. 95–122, May 2020, doi: 10.13104/imri.2020.24.3.95.

[21] O. Ocali and E. Atalar, "Ultimate intrinsic signal-to-noise ratio in MRI," *Magn. Reson. Med.*, vol. 39, no. 3, pp. 462–473, Mar. 1998, doi: 10.1002/mrm.1910390317.

[22] H. Çelik, Y. Eryaman, A. Altintas, I. A. Abdel-Hafez, and E. Atalar, "Evaluation of internal MRI coils using ultimate intrinsic SNR," *Magn. Reson. Med.*, vol. 52, no. 3, pp. 640–649, Sep. 2004, doi: 10.1002/mrm.20200.

[23] C. Coillot, R. Sidiboulenouar, E. Nativel, M. Zanca, E. Alibert, M. Cardoso, G. Saintmartin, H. Noristani, N. Lonjon, M. Lecorre, F. Perrin, and C. Goze-Bac, "Signal modeling of an MRI ribbon solenoid coil dedicated to spinal cord injury investigations," *J. Sensors Sensor Syst.*, vol. 5, no. 1, pp. 137–145, Apr. 2016, doi: 10.5194/jsss-5-137-2016.

[24] O. Dietrich, J. G. Raya, S. B. Reeder, M. F. Reiser, and S. O. Schoenberg, "Measurement of signal-to-noise ratios in MR images: Influence of multichannel coils, parallel imaging, and reconstruction filters," *J. Magn. Reson. Imag.*, vol. 26, no. 2, pp. 375–385, Aug. 2007, doi: 10.1002/jmri.20969.

[25] H. Kovacs, D. Moskau, and M. Spraul, "Cryogenically cooled probes—A leap in NMR technology," *Prog. Nucl. Magn. Reson. Spectrosc.*, vol. 46, nos. 2–3, pp. 131–155, May 2005, doi: 10.1016/j.pnmrs.2005.03.001.

[26] P. Kolar, M. S. Grbić, and S. Hrabar, "Sensitivity enhancement of NMR spectroscopy receiving chain used in condensed matter physics," *Sensors*, vol. 19, no. 14, p. 3064, Jul. 2019, doi: 10.3390/s19143064.

[27] S. Gabriel, R. W. Lau, and C. Gabriel, "The dielectric properties of biological tissues: III. Parametric models for the dielectric spectrum of tissues," *Phys. Med. Biol.*, vol. 41, no. 11, pp. 2271–2293, Nov. 1996, doi: 10.1088/0031-9155/41/11/003.

[28] F. Eggenschwiler, T. Kober, A. W. Magill, R. Gruetter, and J. P. Marques, "SA2RAGE: A new sequence for fast B1+-mapping," *Magn. Reson. Med.*, vol. 67, no. 6, pp. 1609–1619, Jun. 2012, doi: 10.1002/mrm.23145.

[29] G. Helms, H. Dathe, and P. Dechent, "Quantitative FLASH MRI at 3T using a rational approximation of the Ernst equation," *Magn. Reson. Med.*, vol. 59, no. 3, pp. 667–672, Mar. 2008, doi: 10.1002/mrm.21542.

[30] F. Caspers, "RF engineering basic concepts: S-parameters," 2012, *arXiv:1201.2346*.

[31] B. Gruber, M. Froeling, T. Leiner, and D. W. J. Klomp, "RF coils: A practical guide for nonphysicists," *J. Magn. Reson. Imag.*, vol. 48, no. 3, pp. 590–604, Jun. 2018, doi: 10.1002/jmri.26187.

[32] B. Madore and R. M. Henkelman, "A new way of averaging with applications to MRI," *Med. Phys.*, vol. 23, no. 1, pp. 109–113, Jan. 1996, doi: 10.1118/1.597687.

[33] S.-K. Lee, S. Oh, H.-S. Kim, and B.-P. Song, "Radio-frequency vector magnetic field mapping in magnetic resonance imaging," *IEEE Trans. Med. Imag.*, vol. 40, no. 3, pp. 963–973, Mar. 2021, doi: 10.1109/TMI.2020.3043294.

[34] S. Yeo, S. Lee, and S. Lee, "Rapid calculation of static magnetic field perturbation generated by magnetized objects in arbitrary orientations," *Magn. Reson. Med.*, vol. 87, no. 2, pp. 1015–1027, Feb. 2022, doi: 10.1002/mrm.29037.

BYUNG-PAN SONG received the B.S. degree in biomedical engineering from Gachon University, Incheon, Republic of Korea, in 2019, and the M.S. degree in biomedical engineering from Sungkyunkwan University, Suwon, Republic of Korea, in 2022.

His research interest includes RF coils called histology coil development for high-resolution micro-tissue MR microscopy.

HYEONG-SEOP KIM received the B.S. degree in biomedical engineering from Gachon University, Incheon, Republic of Korea, in 2019. He is currently pursuing the M.S. degree in intelligent precision healthcare convergence with Sungkyunkwan University, Suwon, Republic of Korea.

His research interest includes RF coils called human 7T multi-channel RF coil development for high-resolution visual cortex imaging.

SUNG-JUN YOON received the B.S. degree in biomedical engineering from Sungkyunkwan University, Suwon, Republic of Korea, in 2022.

He is currently a Researcher with the Department of Electronic and Electrical Engineering, Sungkyunkwan University. His research interest includes stretchable bio-integrated electronics using soft materials.

DANIEL HERNANDEZ received the Ph.D. degree from Kyung Hee University, Republic of Korea, in 2016.

He has experience working as a Research Professor and an Assistant Professor with the Department of Biomedical Engineering, Gachon University. His research interests include electromagnetic theory, simulations and development of antennas, and image and signal processing for MRI engineering.

KYOUNG-NAM KIM received the Ph.D. degree in electrical engineering and information technology from the University of Duisburg-Essen, Germany, in 2011. He has been an Associate Professor with the Department of Biomedical Engineering, Gachon University, Incheon, Republic of Korea, since 2016. His research interests include medical electronic engineering, MRI systems, electromagnetic field analysis, and RF MRI coils. He is currently a MRI Committee Member of the Korean Society of Magnetic Resonance in Medicine.

SEUNG-KYUN LEE received the Ph.D. degree in physics from UC Berkeley, CA, USA, in 2005. From 2005 to 2008, he was a Postdoctoral Research Associate with the Physics Department, Princeton University. In 2008, he joined the GE Global Research Center, Niskayuna, NY, USA, to develop high-field MRI technologies, where he is currently a Principal Scientist. From 2016 to 2021, he has worked on the Academic Faculty at the Department of Biomedical Engineering and the Department of Intelligent Precision Healthcare Convergence, Sungkyunkwan University, Suwon, South Korea.